IGARSS 2024 - 2024 IEEE International Geoscience and Remote Sensing Symposium | 979-8-3503-6032-5/24/$31.00 ©2024 IEEE | DOI: 10.1109/IGARSS53475.2024.10640563

A DEEP LEARNING APPROACH FOR HIGH-ACCURACY RADIOMETER CALIBRATION USING SMAP SATELLITE DATA

A. M. Alam$^{(1)}$, *M. Kurum*$^{(2)}$, *M. Ogut*$^{(3)}$, *A. C. Gurbuz*$^{(1)}$

(1) Mississippi State University, Mississippi State, MS, USA,
(2) University of Georgia, Athens, GA, USA
(3) Jet Propulsion Laboratory, California Institute of Technology, Pasadena, CA, USA

ABSTRACT

Radiometers play a crucial role in providing accurate geophysical information, relying heavily on precise calibration for both radiometric accuracy and spectral consistency. Radiometers consistently allocate time and hardware resources to calibration, resources that could otherwise be utilized for environmental sensing. In addition, calibration faces challenges such as frequency dependence and environmental influences, requiring to the need for innovative solutions. In this study, advancements in deep learning (DL) techniques are utilized, using NASA's Soil Moisture Active Passive (SMAP) satellite data to create a DL-based radiometer calibrator. The use of 2-D spectral features as input in a convolutional neural network shows promising results with high correlation and low error. Notably, ancillary features like internal thermistor temperature prove accurate for estimating antenna temperature. This compensates for changes in receiver noise temperature and short-term gain fluctuations, even when there's no reference load or noise diode power. The proposed calibration technique, emphasizing reduced reference information, holds significant potential for a higher number of antenna scene observations within a footprint.

Index Terms— Radiometric Calibration, deep learning (DL), machine learning (ML), artificial intelligence (AI), microwave radiometry, neural network, radio frequency interference (RFI), soil moisture active passive (SMAP).

1. INTRODUCTION

Microwave and millimeter-wave radiometry significantly contribute to our understanding of geophysical parameters, such as soil moisture, sea-surface wind, atmospheric water vapor and ocean salinity. These instruments play a vital role in diverse fields like hydrology and meteorology [1–3]. Ensuring their accuracy and sensitivity is crucial for reliable parameter derivation. While accuracy impacts data reliability, sensitivity determines the smallest detectable change, accounting for internal noise.

Microwave radiometers employ various calibration methods to ensure precise and reliable measurements of microwave radiation, enhancing the accuracy of collected data. These calibration techniques fall into two categories: external calibration and internal calibration [4, 5]. External calibration involves using references or targets in space to calibrate the radiometer's measurements, utilizing well-characterized radiometric properties of known targets as references for a voltage-to-antenna temperature calibration line. However, challenges arise, including accessing stable calibration references, environmental variations, instrument stability within the calibration cycle, and correcting fast 1/f noise gain fluctuations. On the other hand, radiometer internal calibration incorporates noise injection and Dicke-switching reference loads. By rapidly switching between internal calibration sources, this technique effectively eliminates gain fluctuations caused by 1/f noise at the receiver output. However, uncertainties may be introduced in the calibration due to factors such as noise diode instability from thermal fluctuations and aging, as well as potential mismatches at the reference load. These factors can lead to errors or biases in the calibration, impacting the accuracy of radiometric measurements.

This paper introduces a novel calibration approach based on deep learning (DL), leveraging 2-D time–frequency spectral features and reduced reference information from reference and noise sources to estimate antenna temperature [6]. The application of convolutional neural network (CNN) based DL framework demonstrates promising potential in minimizing the need for frequent internal calibration, allowing for increased frequency in antenna temperature measurements. Post-launch, samples from vicarious sources or other calibration targets can be used to fine-tune the DL-based calibration during on-orbit operation. This adjustment is crucial in accommodating on-orbit effects and non-stationary instrument changes, such as aging and orbital variations. Data-driven calibration methods have been introduced first in this [7, 8]. This work is centered around using average voltage or antenna temperature. However, with radiometers transitioning to wideband sensing in unprotected regions, there's a growing emphasis on harnessing spectral information. Radiome-

---

This work was supported by National Science Foundation under Grant No. 2332661 and National Aeronautics and Space Administration under Grant No. 80NM0018D0004.

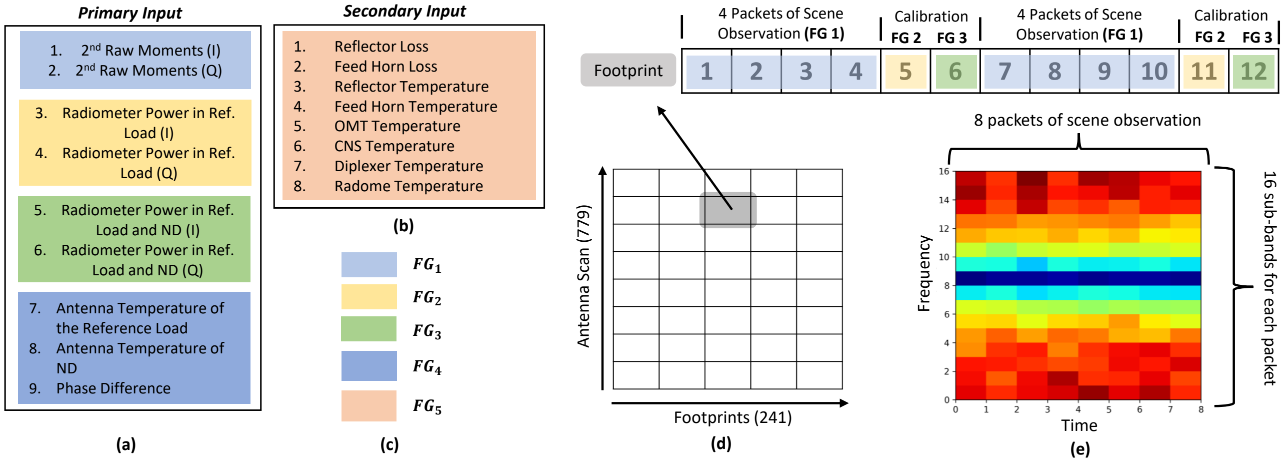

Fig. 1. Illustration of input features for DL-based radiometer calibration. (a) Two-dimensional (16×8) Primary inputs. (b) Scalar secondary inputs. (c) Five feature groups (FG) for different training/testing scenarios illustrated with colors. (d) SMAP data structure for a particular HDF5 file and corresponding switching sequence of a particular footprint. (e) The overall spectrogram of a particular footprint comprises 8 antenna measurements and 16 sub-bands for each antenna measurement [6].

ters capture 2-D time-frequency data, an aspect not directly tapped into by conventional calibration methods. This study introduces an innovative approach that incorporates these 2-D features, along with supplementary ancillary information, for calibration. The goal is to assess the robustness of this approach with reduced reference information, employing various validation strategies to understand the generalization capability of DL in estimating antenna temperature. Future studies will implement this DL-based calibrator in a software-defined radio (SDR)-based L-band radiometer [9].

The remainder of the paper is organized as follows: dataset utilized in this study is detailed in Section 2, while the methodology for DL-based calibration is in Section 3. Results and discussions are provided in Section 4 and finally, a conclusion is drawn in Section 5.

2. DATASET

2.1. SMAP Level 1A Data

The SMAP level 1A data product includes antenna counts at both full-band and subband levels, with these counts being represented by various statistical raw moments [10]. Among these moments, the second raw moments are particularly important as they serve as an equivalent measure of power. In our research, we focus on these second raw moments as the primary input for analysis. Fig. 1a provides a list of features extracted from the level 1A data product, and our input features also encompass the measured counts of the reference load and the reference plus ND. These reference counts offer valuable information and are used alongside the raw antenna moments in our analysis. It's worth noting that all these moments are accessible in both the in-phase (I) and quadrature (Q) channels for both horizontal polarization (H-pol) and vertical polarization (V-pol). This comprehensive set of features forms the basis for our research investigation.

2.2. SMAP Level 1B Data

The level 1B data products include antenna temperature measurements, quality flags indicating data reliability, and details about various radiometer components' loss elements [11, 12]. Fig. 1a and Fig. 1b present these features. In our study, we use the antenna temperature values for both horizontal (H-pol) and vertical polarization (V-pol) as ground truth references. These values help us model the relationship between the measured input voltage and the resulting antenna temperature. To enhance calibration, we incorporate thermistor data from the reference load and ND physical temperature as input features for our model. Additionally, the model includes thermistor/physical temperature readings from different satellite components, such as the reflector, feed horn, orthomode transducer (OMT), and correlated noise source (CNS) during training. Crucial to radiometer calibration are the loss elements of various components, including reflector loss, feed horn loss, and phase imbalances, which are extracted from SMAP level 1B data products. For more in-depth information about these features, refer to the algorithm theoretical basis document of SMAP.

2.3. Data Preparation

The input features for the DL-based calibrator are categorized into primary and secondary groups. Primary inputs include 2-D time–frequency spectrograms fed directly into the convolutional layers of the DL model. Secondary inputs, divided into five feature groups (FGs), are integrated within the DL framework along with primary input features. The five FGs serve various roles in calibrating radiometers, accommodating scenarios with or without power information from the reference and ND. They include features related to the 2nd raw moments (FG1), power of the reference load (FG2), power of ND (FG3), internal physical temperature (FG4), and element losses and physical temperatures (FG5). Radiometer footprints are sequences of 12 packets, each lasting 1.2 ms. FG1 packets focus on observing the scene, while FG2 and FG3 packets are allocated for internal calibration. The data within each packet is divided into 16 subbands covering the SMAP radiometer band of 1400–1427 MHz. The primary inputs, represented by 2-D spectrograms, have a shape of 16 × 8. An example antenna count spectrogram (Fig. 1e) displays eight antenna measurements and 16 subbands within a particular footprint. To maintain a consistent matrix size for the DL model, observations are broadcasted into 16 × 8, involving the extension of the same reference packet for four consecutive packets in a specific subband.

2.4. Training Scenarios

In the previous section, we discussed how input features are categorized into five Functional Groups (FGs) for radiometer calibration. These FGs play a crucial role in creating different training schemes for DL-based frameworks, each aimed at determining the optimal amount of voltage or power information needed from the reference unit to accurately estimate antenna temperature. In these cases, FG_2 and FG_3 represent using only the 5th and 6th time packet observation of FG_2 and FG_3. These schemes are illustrated in Fig. 2. Case 1 aligns with conventional radiometer calibration using the same input features. While a direct comparison with conventional approaches is beyond our study scope, future research will explore applying this calibration method to airborne L-band radiometers for performance comparison. Case 2 uses information from ND without matched reference load information, while Case 3 does the opposite. Case 4 involves using one packet of reference and ND information, unlike conventional calibration requiring two packets per radiometer footprint. Case 5 uses no power information from the reference load and ND. Throughout the training process, FG_1, FG_4, and FG_5 are always incorporated, with FG_4 containing the physical temperature feature of the reference and ND. Our findings suggest that thermistor temperature and loss elements exhibit sufficient stability to compensate for variations in receiver noise temperature and short-term gain fluctuations in the absence of reference load and ND power.

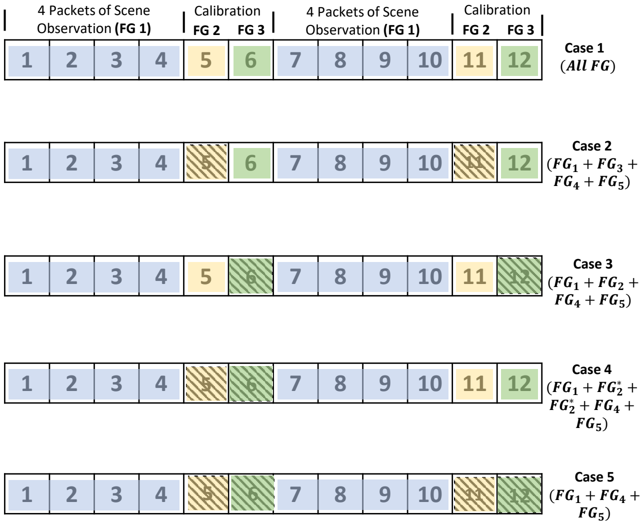

Fig. 2. Different training schemes for DL-based calibrator.

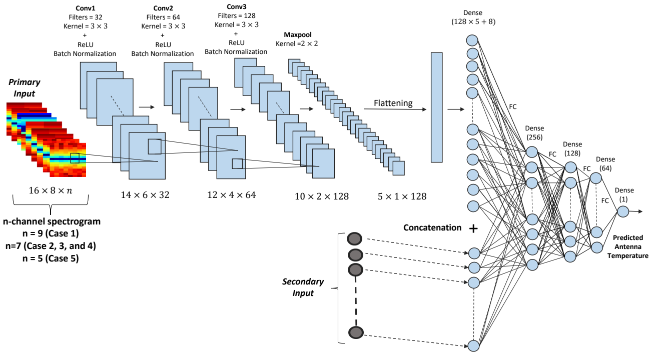

Fig. 3. Deep learning architecture to predict antenna temperature [6].

3. METHODOLOGY

3.1. DL-Based Framework for Calibration

The DL framework, depicted in Fig. 3, comprises convolutional layers for extracting features from n-channel spectrograms, concatenation layers to combine these features with secondary inputs, and densely connected layers for mapping the combined features to radiometer antenna temperature. The primary input is 2-D spectrograms containing data about observation, reference, ND, and phases. To assess the model's flexibility, it's trained and tested under five different scenarios, demonstrating its superiority over conventional forward modeling. Three convolutional layers, using 32, 64, and 128 filters with 3 × 3 kernels and no padding, extract meaningful features from the input spectrograms. Each convolutional layer is followed by ReLU activation and batch normalization, enhancing non linearity and stabilizing distributions for efficient learning. The normalization process in batch normalization minimizes internal covariate shift during training, promoting faster network convergence. With no feature normalization before entering the model, batch normalization aids convergence by reducing the need for careful initialization. A total of 640 features are extracted, flattened, and combined with secondary features. These combined features pass through three fully connected layers (256, 128, and 64 neurons) with ReLU activation, and the last layer, with a linear activation function, produces the final output. The DL model estimates antenna temperature, with input variations based on training scenarios. Ground truth is established using SMAP antenna temperature for a specific footprint. The training optimizes parameters through backpropagation, employing a mean squared error (MSE) loss function that ensures alignment between SMAP-derived ground truth and DL model output. Notably, the model undergoes robust training with a combination of techniques, including learning rate schedulers and early stopping, aiming for a balanced fit to training data and effective generalization to unseen data.

4. RESULTS AND DISCUSSION

4.1. Overall Performance

Two validation techniques, train-test split and K-fold, are utilized with a dataset comprising land and land-water samples. Table 1 summarizes the overall performance in various training-testing scenarios for both land and land-water mixtures. In the train-test split, Case 1 excels with the lowest RMSE values (0.24 K for land, 0.29 K for land-water) and high R^2 values (0.9998 and 0.9997), underlining DL's efficacy with features comparable to conventional radiometers. Case 2, excluding power information, maintains impressive performance (RMSE 0.42 for land, 0.40 for land-water), showcasing DL's ability with minimal reference data. Case 3, incorporating reference plus ND power, outperforms Case 2. Case 4, using a single packet of power information, surpasses Cases 2 and 3. Despite Case 5's decline without reference and ND power, the DL calibrator maintains RMSE (0.67 K land, 0.45 K land-water) below SMAP radiometer uncertainty (1.3K). Training with land-water mix data yields lower RMSE, indicating diverse features. K-fold validation aligns with train-test split, confirming DL's resilience. Case 1 excels, while Cases 2-5 with reduced reference data exhibit low RMSE and high R^2, catering to specific radiometer needs.

4.2. Computational Complexity

This study introduces a DL framework for predicting SMAP radiometer antenna temperature, considering diverse spatial and temporal data distributions. The quantitative analysis focuses on determining the required amount of data for prediction. Fig. 4 illustrates RMSE performance for varying training sizes across five cases, with a fixed SMAP radiometer uncertainty line at 1.3 K. Generally, RMSE decreases with larger training sizes. Notably, Cases 1 and 4 achieve acceptable RMSE with only 25% of the training dataset, while Cases 2 and 3 require around 40%. Case 5 needs approximately 60%. Cases 1 and 4 benefit from power features, aiding quick convergence, while Cases 2 and 3, with less reference information, demand more training samples. Overall, the DL-based calibrator demonstrates satisfactory performance even with reduced reference information and training data.

Table 1. Performance Metrics of DL-based Calibrator with Train-Test Split and K-Fold

Validation Techniques	Training Scenarios	Land		Land and Water	
		RMSE (K)	R^2	RMSE (K)	R^2
Train-Test Split	Case 1	0.24	0.9998	0.29	0.9997
	Case 2	0.42	0.9994	0.40	0.9995
	Case 3	0.43	0.9994	0.37	0.9996
	Case 4	0.35	0.9996	0.33	0.9996
	Case 5	0.67	0.9991	0.45	0.9993
K-Fold	Case 1	0.27	0.9997	0.31	0.9997
	Case 2	0.45	0.9993	0.41	0.9994
	Case 3	0.47	0.9992	0.40	0.9994
	Case 4	0.37	0.9996	0.36	0.9996
	Case 5	0.72	0.9990	0.51	0.9992

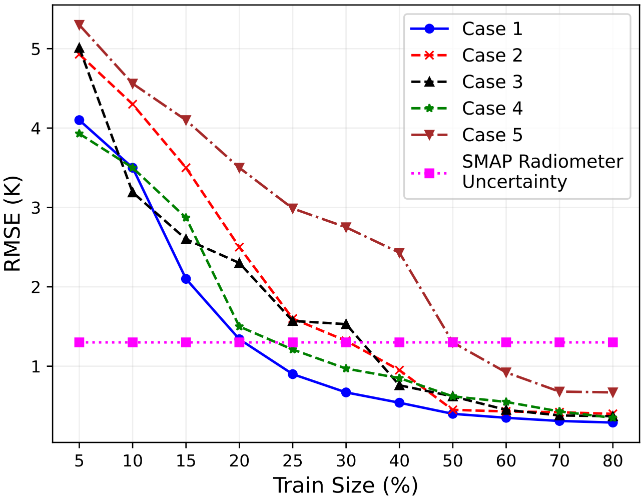

Fig. 4. Comparing RMSE Errors of Various Training Scenarios with SMAP Radiometer Uncertainty.

5. CONCLUSION

This research highlights the effectiveness of calibrating radiometers through the use of DL techniques. It takes advantage of limited reference information and organizes two-dimensional antenna counts into time and frequency sub-bands. This DL-based calibrator will play a vital role in a future end-to-end data-driven microwave radiometer setup. It will be integrating seamlessly into a framework that includes a pre-existing unit for detecting and mitigating radio frequency interference [13–15].

6. REFERENCES

[1] N. Grody, "Remote Sensing of Atmospheric Water Content From Satellites Using Microwave Radiometry," *IEEE Transactions on Antennas and Propagation*, vol. 24, no. 2, pp. 155–162, 1976.

[2] D. M. Le Vine, A. J. Griffis, C. T. Swift, and T. J. Jackson, "ESTAR: A Synthetic Aperture Microwave Radiometer For Remote Sensing Applications," *Proceedings of the IEEE*, vol. 82, no. 12, pp. 1787–1801, 1994.

[3] C. S. Ruf, C. T. Swift, A. B. Tanner, and D. M. Le Vine, "Interferometric Synthetic Aperture Microwave Radiometry for the Remote Sensing of the

Earth," *IEEE Transactions on Geoscience and Remote Sensing*, vol. 26, no. 5, pp. 597–611, 1988.

[4] F. T. Ulaby, R. K. Moore, and A. K. Fung, "Microwave Remote Sensing: Active and Passive. Volume 1 - Microwave Remote Sensing Fundamentals and Radiometry," 1981.

[5] J. R. Piepmeier, P. Focardi, K. A. Horgan, J. Knuble, N. Ehsan, J. Lucey, C. Brambora, P. R. Brown, P. J. Hoffman, R. T. French, R. L. Mikhaylov, E.-Y. Kwack, E. M. Slimko, D. E. Dawson, D. Hudson, J. Peng, P. N. Mohammed, G. De Amici, A. P. Freedman, J. Medeiros, F. Sacks, R. Estep, M. W. Spencer, C. W. Chen, K. B. Wheeler, W. N. Edelstein, P. E. O'Neill, and E. G. Njoku, "SMAP L-Band Microwave Radiometer: Instrument Design and First Year on Orbit," *IEEE Transactions on Geoscience and Remote Sensing*, vol. 55, no. 4, pp. 1954–1966, 2017.

[6] A. M. Alam, M. Kurum, M. Ogut, and A. C. Gurbuz, "Microwave radiometer calibration using deep learning with reduced reference information and 2-d spectral features," *IEEE Journal of Selected Topics in Applied Earth Observations and Remote Sensing*, vol. 17, pp. 748–765, 2024.

[7] M. Ogut, X. Bosch Lluis, and S. C. Reising, "A Deep Learning Approach for Microwave and Millimeter-Wave Radiometer Calibration," *IEEE Transactions on Geoscience and Remote Sensing*, vol. 57, no. 8, pp. 5344–5355, 2019.

[8] M. Ogut, X. Bosch-Lluis, and S. C. Reising, "Deep Learning Calibration of the High-Frequency Airborne Microwave and Millimeter-Wave Radiometer (HAMMR) Instrument," *IEEE Transactions on Geoscience and Remote Sensing*, vol. 58, no. 5, pp. 3391–3399, 2020.

[9] A. M. Alam, M. M. Farhad, M. Kurum, and A. Gurbuz, "An advanced testbed for passive/active coexistence research: A comprehensive framework for rfi detection, mitigation, and calibration," in *2024 United States National Committee of URSI National Radio Science Meeting (USNC-URSI NRSM)*, 2024, pp. 280–280.

[10] J. R. Piepmeier, E. J. Kim, P. Mohammed, J. Peng, and C. Ruf, "SMAP L1A Radiometer Time-Ordered Parsed Telemetry, Version 2," *Nat. Snow Ice Data Center, Boulder, CO, USA*, 2015.

[11] J. R. Piepmeier, P. Mohammed, J. Peng, E. J. Kim, G. De Amici, J. Chaubell, and C. Ruf, "SMAP L1B Radiometer Half-Orbit Time-Ordered Brightness Temperatures, Version 5," *Nat. Snow Ice Data Center, Boulder, CO, USA*, 2020.

[12] J. Piepmeier, P. Mohammed, G. De, A. E. Kim, J. Peng, and C. Ruf, "Soil Moisture Active Passive (SMAP) Algorithm Theoretical Basis Document (ATBD) SMAP Calibrated, Time-Ordered Brightness Temperatures L1B TB Data Product," 2014.

[13] A. M. Alam, M. Kurum, and A. C. Gurbuz, "High-Resolution Radio Frequency Interference Detection in Microwave Radiometry Using Deep Learning," in *IGARSS 2023 - 2023 IEEE International Geoscience and Remote Sensing Symposium*, 2023, pp. 6779–6782.

[14] A. M. Alam, A. C. Gurbuz, and M. Kurum, "SMAP Radiometer RFI Prediction with Deep Learning using Antenna Counts," in *IGARSS 2022 - 2022 IEEE International Geoscience and Remote Sensing Symposium*, 2022, pp. 8016–8019.

[15] A. M. Alam, M. Kurum, and A. C. Gurbuz, "Radio Frequency Interference Detection for SMAP Radiometer Using Convolutional Neural Networks," *IEEE Journal of Selected Topics in Applied Earth Observations and Remote Sensing*, vol. 15, pp. 10 099–10 112, 2022.